HHS Public Access

Author manuscript

Nat Neurosci. Author manuscript; available in PMC 2013 April 01.

Published in final edited form as:

Nat Neurosci. 2012 October ; 15(10): 1414–1421. doi:10.1038/nn.3209.

Calcium entry induces mitochondrial oxidant stress in vagal neurons at risk in Parkinson's disease

Joshua A. Goldberg, **Jaime N. Guzman**, **Chad M. Estep**, **Ema Ilijic**, **Jyothisri Kondapalli**, **Javier Sanchez-Padilla**, and **D. James Surmeier**

Department of Physiology, Feinberg School of Medicine, Northwestern University Chicago, Illinois, 60611 USA

Abstract

Mitochondrial oxidant stress is widely viewed as critical to pathogenesis in Parkinson's disease. But the origins of this stress are poorly defined. One possibility is that it arises from the metabolic demands associated with regenerative activity. To test this hypothesis, neurons in the dorsal motor nucleus of the vagus (DMV), a population cholinergic neurons that shows signs of pathology in the early stages of Parkinson's disease, were characterized in mouse brain slices. DMV neurons were slow, autonomous pacemakers with broad spikes, leading to calcium entry that was weakly buffered. Using a novel transgenic mouse expressing a redox-sensitive optical probe targeted to the mitochondrial matrix, it was found that calcium entry during pacemaking created a basal mitochondrial oxidant stress. Knocking out *DJ-1* – a gene associated with early-onset Parkinson's disease – exacerbated this stress. These results point to a common mechanism underlying mitochondrial oxidant stress in Parkinson's disease and a therapeutic strategy to ameliorate it.

Keywords

L-type calcium channel; electrophysiology; roGFP; neurodegeneration; dihydropyridine; neuroprotection; multiphoton imaging; *DJ-1*; *Park7*; calcium buffering protein; calcium buffering capacity

Introduction

Parkinson's disease is the second most common neurodegenerative disease[1]. Nothing is known to slow its inexorable progression. As a consequence, there has been a concerted effort to understand its pathogenic mechanisms. Many lines of study ranging from the

Corresponding author: D. James Surmeier, Department of Physiology, Feinberg School of Medicine, Northwestern University, 303 E. Chicago Ave. Chicago, IL, 60611, j-surmeier@northwestern.edu, Tel. 1-312-503-4904.

Competing financial interests

The authors declare no competing financial interests.

Author contributions: J.A.G. designed and conducted experiments and analyzed the data; J.N.G. conducted some of the control roGFP experiments; C.M.E. and E.I. conducted the histological experiments; J.K. and J.S-P. generated the CMV-mito-roGFP and the *DJ-1*$^{-/-}$ mice; D.J.S. was responsible for the overall direction of the experiments. J.A.G and D.J.S. prepared the manuscript and illustrations.

functional analysis of genetic mutations in rare familial forms of Parkinson's disease to the characterization of postmortem tissue from Parkinson's disease patients point to mitochondrial oxidant stress as a key step in the cascade of events leading to degeneration[2–4].

As compelling as the mitochondrial theory of pathogenesis is, it does not explain the pattern of neuronal pathology and degeneration in Parkinson's disease. The cardinal motor symptoms of Parkinson's disease are largely attributable to the degeneration of a small group of dopaminergic neurons in the substantia nigra pars compacta (SNpc)[5]. However, it has become clear that the pathology in Parkinson's disease is more widespread, encompassing a variety of small, scattered nuclei in the brainstem and olfactory system in the early stage of the disease[6]. The most obvious sign of pathology in these nuclei is the presence of proteinaceous intracellular inclusions called Lewy bodies or Lewy neurites (LBNs)[7, 8]. Neurons in the dorsal motor nucleus of the vagus (DMV) in the caudal medulla are thought to be among the most vulnerable of this group, showing LBN pathology in the early stages of Parkinson's disease[7].

Why should these scattered clusters of neuron be vulnerable to the pathogenic processes in Parkinson's disease and is there evidence that they have mitochondrial dysfunction or stress? Recent examination of SNpc dopaminergic neurons suggests that self-generated neural activity could create a metabolic stress that elevates the sensitivity to mitochondrial toxins and genetic mutations associated with familial forms of Parkinson's disease[9, 10]. SNpc neurons are slow, autonomous pacemakers with broad spikes[11]. Pacemaking is accompanied by sustained calcium entry through L-type voltage-dependent channels[12–14] that is only weakly buffered by cellular binding proteins[15]. Calcium entry through L-type channels leads to increased mitochondrial oxidant stress; this stress is exacerbated by deletion of DJ-1 – loss of function mutations in DJ-1 are associated with an early onset form of Parkinson's disease[12, 16].

What is less clear is whether other neurons that display LBN pathology in the early stages of Parkinson's disease share this physiological phenotype. To answer this question, we examined cholinergic neurons in the DMV. As noted above, these neurons are among the first to show LBN pathology in Parkinson's disease. Moreover, they regulate a variety of parasympathetic functions, including gastrointestinal motility, which is impaired in many Parkinson's disease patients[17, 18]. Our studies revealed that cholinergic DMV neurons exhibited a slow autonomous pacemaking, broad spike and robust calcium entry through L-type and other calcium channels. Moreover, calcium entering the cytosol was only weakly buffered by endogenous proteins. Using a transgenic mouse that expressed a mitochondrially targeted, redox-sensitive variant of green fluorescent protein (mito-roGFP), we found that spike rate, spike duration and calcium entry through L-type channels all factored into elevating mitochondrial oxidant stress in these neurons. Lastly, mitochondrial oxidant stress was exacerbated in DMV neurons from *DJ-1*$^{-/-}$ mice, and L-type channel antagonists effectively ameliorated this stress – suggesting a common phenotype that defines neurons at risk in Parkinson's disease and a common therapy to protect them.

Results

DMV neurons were autonomous pacemakers with broad spikes

The DMV is situated near the midline, dorsal to the darker and more fibrous hypoglossal nucleus and ventral to the nucleus of the solitary tract (Fig. 1a). To allow the key experimental variables to be controlled, DMV neurons were studied in transverse slices of the medulla oblongata taken from young adult mice. In choline acetyltransferase-enhanced green fluorescent protein (ChAT-eGFP) BAC transgenic mice, the overwhelming majority of DMV neurons were fluorescent allowing their definitive identification as cholinergic neurons. In agreement with previous studies[19], these neurons had 2–4 primary dendrites and an axon that coursed ventrolaterally (Fig. 1b). Perforated patch recordings from these neurons revealed them to be spontaneously active (Fig. 1c), in agreement with previous work in vitro[20, 21]. The spontaneous spikes were broad (2.7 ± 0.1 ms, $n = 34$) (Fig. 1d), much like those of SNpc dopaminergic neurons. The slow spontaneous spiking (Fig. 1e) was autonomously generated, as a cocktail of glutamatergic, GABAergic, cholinergic, serotonergic and adrenergic receptor antagonists failed to significantly alter its rate [1.6 ± 0.2 spikes per second in ACSF vs. 1.6 ± 0.2 spikes per second in blockers, $P > 0.3$, two-tailed Wilcoxon signed-rank test (SRT) for paired samples, $n = 40$].

As in SNpc dopaminergic neurons, the sub-threshold voltage trajectory during this slow spiking was restricted to a relatively depolarized voltage range (−65 mV to −40 mV). The mechanisms necessary to generate slow autonomous pacemaking within this voltage range are reasonably well-defined[22]. The most fundamental requirement is that the cell must not possess a stable membrane potential below spike threshold. In most pacemaking neurons, inward, depolarizing currents carried by voltage-dependent sodium and hyperpolarization/cyclic nucleotide gated (HCN) cation channels destabilize the membrane potential[22, 23]. In DMV neurons, the Nav1 sodium channel blocker tetrodotoxin (TTX, 1 μM) stopped autonomous spiking and eliminated sub-threshold oscillations in voltage, creating a stable resting potential (Fig. 2a). Voltage-clamp measurements of the TTX-sensitive Nav1 channel currents in the soma revealed that these channels had a prominent persistent opening mode that was evident at membrane potentials at and above −60 mV (Fig. 2b), as in other pacemaking neurons[22, 23]. As reported previously[21], HCN channel currents were also evident in this voltage range. However, HCN channel density varied considerably and only about half the neurons tested (33/65) responded to negative current steps by initially hyperpolarizing and then slowly depolarizing (or sagging); this depolarization is a manifestation of HCN channel activation by hyperpolarization. As further evidence of this variability, the HCN channel antagonist ZD 7288 (20 μM) slowed pacemaking in only 3 of 7 neurons, leaving the rest unaffected (Supplementary Fig. 1).

Another channel that supports pacemaking is the voltage-insensitive cation channel NALCN[23, 24]. NALCN channel mRNA was robustly expressed in DMV neurons (Fig. 2c). This mRNA was translated into functional protein as replacing extracellular sodium with the larger membrane impermeable cation N-methyl-D-glucamine (NMDG) led to a substantial hyperpolarization of the membrane potential in the presence of TTX (median hyperpolarization: 17.7 mV, $n = 6$, $P < 0.05$, SRT) (Fig. 2d). These results demonstrate that

pacemaking in DMV neurons depends upon a combination of Nav1, NALCN and to a lesser extent HCN channels.

Pacemaking elevated intracellular calcium concentration

In SNpc dopaminergic neurons, low-threshold L-type calcium channels with a Cav1.3 pore-forming subunit make a significant contribution to the inward currents driving pacemaking[12, 14, 25]. When Nav1 channels are blocked in these cells to eliminate spikes, the Cav1.3 channels generate slow oscillatory potentials (SOPs)[13]. SOPs were not evident in DMV neurons (Fig. 2a), suggesting that Cav1.3 channels play a less significant role. To explore this issue, we measured the somatic membrane was voltage-clamped and the cobalt-sensitive calcium channel currents evoked by the normal pacemaking voltage trajectory[22]. These experiments revealed the presence of a calcium channel current during the sub-threshold portion of the trajectory in most neurons, but this current was relatively small, amounting to a few tens of picoamperes (Fig. 3a). Comparing this calcium current to the TTX-sensitive sodium currents over the same sub-threshold voltage range reinforced this point (Fig. 3b). The only voltage-dependent calcium channel capable of sustained activation in this voltage range is an L-type channel with a Cav1.3 pore-forming subunit[26, 27].

The expression of mRNA for the Cav1.3 subunit in DMV neurons was verified by single-cell RT-PCR. This analysis also revealed robust expression of the high-voltage activated Cav1.2 subunit (Fig. 3c). These channels, along with other high-voltage activated channels, contribute to the calcium currents evoked by the spike itself. These currents in DMV neurons were large, constituting 0.5–2.9 picocoulombs (n = 14, data not shown) per spike (Fig. 3d). The broad, slow spikes of DMV neurons were undoubtedly a contributing factor in this calcium entry. To chart the relationship between spike width and calcium entry, the somatic voltage was clamped to temporally scaled versions of the spike (ranging from a tenth to twice the physiological width). This analysis revealed a remarkably linear relationship between spike duration and the amount of calcium that entered the cell (n = 5 cells) (Fig. 3d).

To complement these studies, we used two-photon laser scanning microscopy (2PLSM) to monitor intracellular calcium concentration in DMV neurons dialyzed with calcium dye Fluo-4 (100 μM). During normal pacemaking, intracellular calcium concentration rose rapidly following the spike and then fell exponentially during the interspike interval (Fig. 4a,b). Abolishing spikes with TTX eliminated the fluctuations in intracellular calcium concentration (Fig. 4a), providing additional evidence against a sub-threshold, calcium channel dependent oscillation. Manipulating spike rate by intracellular current injection demonstrated that spike rate was the primary determinant of free cytosolic calcium concentration in DMV neurons (Fig. 4c).

Precisely which channels are responsible for the high-threshold, spike evoked calcium currents in DMV neurons? Previous work has implicated both Cav1 and Cav2 channels[28, 29]. Cav2.2 channel currents were reported to exert a strong effect on the medium duration after-hyperpolarization (mAHP) mediated by the small-conductance, calcium-activated (SK) potassium channel[29]. As predicted, the Cav2.2 antagonist ω-conotoxin GVIA (1 μM) reduced the mAHP, resulting in a significant acceleration in pacemaking rate

(Supplementary Fig. 2a). Blocking SK channels directly with the bee venom apamin (100 nM) also reduced the mAHP and accelerated pacemaking more dramatically (Supplementary Fig. 2b). In contrast, antagonizing L-type channels with either isradipine (200 nM) or calciseptine (200 nM) had no effect on basal pacemaking rate (Kruskal-Wallis one-way ANOVA, dof = 77, $\kappa^2 = 0.86$, $P > 0.6$) (Fig. 5a), but did reduce the slow after-hyperpolarization potential (sAHP) evoked by a burst of spikes (median decrease: 6.9 mV, $n = 7$, $P < 0.05$, SRT) (Fig. 5b), as reported previously[29]. Although they had little effect on the rate of regular spiking, L-type channels did contribute to intracellular calcium concentration during this activity mode as antagonizing them significantly diminished Fluo-4 fluorescence ($n = 10$, $P < 0.01$, SRT) (Fig. 5c). Thus, while both Cav1 and Cav2 channels enable calcium entry during spikes, the rate of spiking appears to be most directly controlled by Cav2 channels, making them undesirable therapeutic targets.

DMV neurons had a low intrinsic buffering capacity

A potentially important determinant of vulnerability in Parkinson's disease is the expression of calcium binding proteins (CaBPs) that provide an energy neutral means of buffering intracellular calcium[30]. DMV neurons have not been reported to express detectable levels of either calbindin or parvalbumin, two common CaBPs[29, 31]. However, it is possible that they express some other, less well-characterized CaBPs. To test this possibility, we estimated the intrinsic buffering capacity of DMV neurons using the "added buffer" method[32]. We derived a formalism to estimate the exogenous incremental buffering capacity κ'_B[33] when using a high dynamic range, non-ratiometric calcium indicator, like Fluo-4 (See eq. [5] in Online Methods). To estimate κ'_B, calcium influx was evoked with a spike as the indicator filled the cell. The indicator concentration as a function of time, which is the main determinant of κ'_B, was estimated by fitting an exponential curve to pre-spike fluorescence, F_0 (Fig. 6a). As expected, the relative amplitude of the evoked fluorescence signal decreased and its decay time-constant increased as the cell filled with the exogenous buffer (Fig. 6b)[32, 34]. By fitting the binding isotherm that relates the change in raw fluorescence (ΔF) to κ'_B, the endogenous buffering capacity of the cell (κ_s) was estimated (Fig. 6c). The median κ_s of DMV neurons was 49 ($n = 8$); this means that roughly 2 ions of every 100 calcium ions entering the cell are unbound. This κ_s value is very low for neurons and close to that of other neurons that are prone to degeneration (e.g., spinal motoneurons[35] and SN dopaminergic neurons[15]). In contrast, the endogenous buffering capacity of VTA dopaminergic neurons ($n = 6$), which are known to express calbindin and to be relatively resistant to degeneration, was a factor of 3 greater [$P < 0.005$, two-tailed Wilcoxon rank-sum test (RST) for independent samples] (Fig. 6d).

Activity-dependent calcium entry oxidized mitochondria

The combination of autonomous pacemaking, depolarized voltage trajectory, broad spikes, robust calcium entry and low calcium buffering capacity could create a metabolic stress on DMV neurons much like that found in SNpc dopaminergic neurons. To test this prediction, we generated transgenic mice expressing a mitochondrial matrix targeted, redox-sensitive variant of green fluorescent protein (mito-roGFP) under control of the cytomegalovirus (CMV) promoter. Previous work with the mito-roGFP construct driven by the tyrosine hydroxylase promoter demonstrated the efficacy of the mitochondrial matrix targeting of

this construct[12]. In these CMV-mito-roGFP mice, DMV neurons robustly expressed mito-roGFP and the construct had a subcellular distribution similar to that of the TH-mito-roGFP mice[12] (Fig. 7a). This provided a means of measuring oxidation of mitochondrial matrix thiol proteins in pacemaking DMV neurons. Using 2PLSM approaches in brain slices, the fluorescence of mito-roGFP was measured; for every neuron, the fluorescence was calibrated at the end of the experiment with strong oxidizing and reducing agents to allow correction for variation in expression level of the probe or optics[12]. As hypothesized, the matrix of mitochondria in most DMV neurons was relatively oxidized (Fig. 7b). Isradipine (200 nM) (Fig. 7c) diminished mitochondrial oxidant stress ($n = 9$, $P < 0.005$, RST), without altering spiking or pacemaking frequency, pointing to the importance of calcium entry in creating it.

Because spike rate and spike duration were major determinants of cytosolic calcium levels in DMV neurons, we hypothesized that manipulating them would affect the oxidation of mitochondrial oxidant stress. This hypothesis was confirmed by experiment. First, antagonizing Nav1 channels with TTX, which eliminates spiking and calcium entry into DMV neurons, significantly diminished mitochondrial oxidant stress ($n = 10$, $P < 0.005$, SRT). Second, lowering the temperature of the bath significantly reduced the firing of DMV neurons [2.39 ± 0.37 spikes per second at 32 °C, $n = 58$, vs. 1.28 ± 0.15 spikes per second at 22 °C, $n = 58$, $P < 0.05$, RST) and diminished mitochondrial oxidant stress (n=5, p<0.05, RST). Third, increasing spike duration by 50% ($n = 6$, $P < 0.05$, SRT) (Fig. 7d) with 0.5 mM tetraethylammonium (TEA) [an antagonist of the large conductance voltage- and calcium-activated (BK) potassium channel)][36] resulted in a significant increase in mitochondrial oxidant stress ($n = 19$, $P < 0.05$, RST) (Fig. 7e). Although TEA broadened the spike, it did not change spike rate (data not shown). Thus, spike duration and rate – the primary determinants of calcium entry into DMV neurons – determine the level of mitochondrial oxidant stress in DMV neurons.

Mitochondrial oxidant stress was exacerbated in DJ-1$^{-/-}$ mice

Mutations in *DJ-1* are linked to an autosomal recessive early-onset form of Parkinson's disease[37]. DJ-1 helps to orchestrate mitochondrial oxidant defenses[37], making its loss of potential importance to metabolically challenged neurons. For example, SNpc dopaminergic neurons lacking the *DJ-1* gene have a higher basal level of mitochondrial oxidant stress[12]. Relieving the metabolic burden on these cells by antagonizing L-type channels normalizes mitochondrial oxidant stress levels. To determine if the metabolic burden on DMV neurons created a similar dependence upon DJ-1, *DJ-1*$^{-/-}$ mice were crossed with CMV-mito-roGFP mice. In DMV neurons from these mice, basal pacemaking was normal in rate (Fig. 7f). Spike width was also normal (data not shown). However, basal mitochondrial oxidant stress levels were elevated in DMV neurons ($n = 7$, $P < 0.05$, RST). Furthermore, as in SNpc dopaminergic neurons, this basal mitochondrial stress was ameliorated by preincubation with isradipine (200 nM) ($n = 9$, $P < 0.05$, RST) (Fig. 7g).

Discussion

The studies presented demonstrate that DMV cholinergic neurons have a physiological phenotype that results in basal mitochondrial oxidant stress. The core elements of this physiological phenotype are slow autonomous pacemaking, broad spikes, calcium entry through voltage-dependent ion channels and modest intrinsic calcium buffering capacity. Antagonizing one of the primary contributors to calcium entry during pacemaking, L-type calcium channels, led to a significant reduction in mitochondrial oxidant stress without altering ongoing activity of DMV cholinergic neurons. Antagonizing L-type channels also ameliorated the elevation in mitochondrial oxidant stress created by deletion of DJ-1, a gene associated with familial forms of Parkinson's disease. The similarities between DMV cholinergic and SNpc dopaminergic neurons suggest that there is a common neuronal phenotype underlying neurodegenerative risk in Parkinson's disease. Moreover, because L-type channel antagonists with good brain bioavailability are well tolerated by humans, our results suggest that their use in early stages Parkinson's disease could slow the evolution of both motor and non-motor symptoms.

The DMV neurons had features common to pacemakers

Pacemaking in DMV neurons relied upon ionic mechanisms shared with other pacemaking neurons that have been characterized in depth. For example, in DMV neurons TTX-sensitive, voltage-dependent sodium channels were critical to the generation of rhythmic membrane potential oscillations and pacemaking, as in many other neurons[22, 23]. Voltage-dependent HCN and voltage-independent NALCN cation channels contributed to the inward currents driving pacemaking in DMV neurons, as in a number of other slow pacemaking neurons[23, 38].

Voltage-dependent, L-type calcium channels also contributed to the inward currents driving pacemaking in DMV cholinergic neurons. However, like the situation in VTA dopaminergic neurons, these currents were substantially smaller than voltage-dependent sodium channel currents[23]. The channels underlying these sub-threshold currents are highly likely to have a Cav1.3 pore-forming subunit[25, 26]. The mRNA coding for this subunit, as well as mRNA for the high threshold Cav1.2 subunit was readily detected in single DMV neurons.

However, the calcium currents evoked by spikes were clearly larger than the sub-threshold currents estimated with somatic point clamp experiments. The broad spikes of DMV neurons enhanced calcium entry through both Cav1 channels and Cav2 channels, leading to the monotonic rise in intracellular calcium concentration with spike rate. Although the voltage-dependence of dihydropyridine binding prevented an accurate estimate of the contribution of L-type channels to the calcium influx during a single spike[39], their contribution to basal intracellular calcium concentration during pacemaking could be estimated by silencing neurons in the presence and absence dihydropyridine; these experiments suggested that L-type channels were responsible for roughly half of the free calcium in the somatic cytoplasm during pacemaking.

Somewhat surprisingly, antagonism of L-type channels generically did not have a significant effect on the overall pacemaking rate. In part, this is attributable to compensatory ionic

mechanisms. In SNpc dopaminergic neurons, where Cav1.3 channel currents are relatively larger, their antagonism does not significantly affect pacemaking either, largely because their antagonism also reduces the opening of SK channels, leading to little net change in transmembrane current[26].

Calcium entry promoted mitochondrial oxidant stress

As in SNpc dopaminergic neurons[12], mitochondrial matrix proteins in DMV neurons exhibited signs of oxidant stress during pacemaking. This measurement was made possible by expression of the reversible, ratiometric redox probe roGFP with a mitochondrial matrix targeting sequence[40]. The expression of the probe was driven by the cytomegalovirus (CMV) promoter, yielding widespread and robust neuronal expression in the brain. Although our experiments did not take advantage of the ratiometric capabilities of roGFP, the optical signal was calibrated at the end of every experiment by washing on strong oxidizing and reducing agents. This allowed us to eliminate effects of expression level or optics and compare the relative redox status of neurons in different conditions.

The mitochondrial oxidant stress in DMV neurons was activity-dependent. Spikes and the concomitant dissipation of ionic gradients increases ATP use in neurons, diminishing their respirator reserve capacity[41]. Calcium entry poses an additional metabolic burden because of the steep electrochemical gradient against which it must be pumped by ATP-dependent mechanisms[9]. The combination of pacemaking, broad spikes and robust calcium channel expression appears to create a substantial metabolic challenge for DMV neurons. That said, VTA dopaminergic neurons show no signs of mitochondrial oxidant stress, in spite of their similar pacemaking phenotype[12]. What distinguishes DMV and VTA neurons is the expression of calcium binding proteins. VTA neurons express high levels of the buffering protein calbindin, leading to estimates of intrinsic calcium buffering capacity in excess of 150. In contrast, DMV cholinergic neurons had much lower intrinsic buffering capacity. Why might this be important? In the absence of fixed calcium buffering proteins, like calbindin and parvalbumin, the burden of maintaining cytosolic calcium homeostasis falls more definitively upon ATP-dependent pumps in the plasma membrane and intracellular organelles, like the endoplasmic reticulum. The ability of calcium to diffuse away from the plasma membrane means that much of the calcium is likely to be pumped into ‘intermediate’ organelle storage sites and then released back into the cytoplasm for eventual extrusion out of the cell[30]. While this allows calcium to perform signaling functions, it inescapably adds to its metabolic cost.

What is less clear is why this increases mitochondrial oxidant stress. Neurons depend upon mitochondria and oxidative phosphorylation to meet their considerable metabolic needs[41]. Neurons cannot survive on glycolysis alone. However, the relationship between oxidative phosphorylation and oxidant stress in the mitochondrion is incompletely understood. It also is not clear how neurons balance mitochondrial mass and regulation of respiratory rate in individual mitochondria to meet their metabolic demands. Calcium appears to be a key regulator of this bioenergetic decision making process, as it not only controls the spatial distribution of mitochondria[42], but also their respiratory rate[43]. Whether L-type calcium channels play a privileged role in this regulatory process remains to be determined.

Implications for the treatment of Parkinson's disease

Impaired gastrointestinal motility is common in Parkinson's disease patients and this could be due to diminished outflow from DMV neurons[17, 18]. This inference is consistent with the prominent LBN pathology and neuronal loss in the DMV of Parkinson's disease brains[7]. As outlined above, the origins of this vulnerability have been unclear. An idea advanced early on by Braak was that vulnerable neurons had long unmyelinated axons that created a metabolic burden, resulting ultimately in bioenergetic deficits, proteostatic dysfunction and LBN pathology[7, 44]. Indeed, many of the neurons that are vulnerable in Parkinson's disease have long, richly branching axons (e.g., SNpc, locus ceruleus, raphe neurons). Our results and the available physiological literature[9] suggest that this anatomical trait is correlated with a physiological phenotype that adds to the metabolic burden these neurons have to carry. This metabolic hypothesis also links mitochondria to pathogenesis. As stated at the outset, many lines of evidence implicate mitochondrial dysfunction in Parkinson's disease[4]. As neurons depend upon mitochondria to meet their bioenergetic needs, it is not surprising that deficits in their ability to generate ATP could lead to neurodegeneration[41]. What has been lacking is an explanation of why some neurons and not others should be susceptible to modest impairments in mitochondrial function. The demonstration that the physiological phenotype of vulnerable neurons results in sustained mitochondrial oxidant stress fills this gap. Over decades, this oxidant stress could lead to mitochondrial decline, bioenergetic deficits, compromised ATP-dependent proteostatic function (resulting in LBN pathology) and ultimately death. Genetic mutations that further compromise mitochondria viability (e.g., DJ-1, Pink1 mutations) or add to the proteostatic workload (e.g., alpha synuclein over-expression) accelerate this decline.

From the clinical standpoint, the question is how can this process be slowed or stopped without compromising neuronal function? Certainly, reducing the axonal projections of vulnerable neurons is not an option. Attempts to directly target mitochondrial function have not been successful to date[45]. Our results point to another therapeutic path. Diminishing activity-dependent calcium entry through L-type channels with dihydropyridines reduced signs of mitochondrial oxidant stress in DMV cholinergic neurons without altering their autonomously generated activity. These compounds have been used safely in humans for decades to treat hypertension and their use is associated with a reduced risk of developing Parkinson's disease[46–48]. Our results suggest that this reduction in risk is not just attributable to an effect on SNpc neurons[12], but to an effect on DMV neurons as well, raising the possibility that a single therapeutic agent might delay the onset of both motor and non-motor symptoms in Parkinson's disease. Whether antagonism of L-type channels can slow the progression of the disease once patients have become symptomatic is uncertain. Recent epidemiological work failed to find a significant effect of dihydropyridine use on time to reach late stage milestones in Parkinson's disease patients[49]. It could be that at this stage other factors, like inflammation[50], begin to drive pathogenesis, diminishing the neuroprotective value of dihydropyridines. It could also be that because neurons are compromised at this stage in the disease, a greater degree of L-type channel antagonism is necessary to achieve protection. In toxin models of Parkinson's disease (where inflammation is a factor), roughly half of the Cav1.3 L-type channels need to be antagonized to achieve any significant level of protection in the SNpc[16]; this level of antagonism is greater than that

achievable with dihydropyridines because of their preference for Cav1.2 channels in the cardiovascular system, pointing to the need for Cav1.3 channel selective antagonists.

Online Methods

Slice Preparation

Experimental procedures adhered to the Northwestern University Animal Care and Use Committee. Three to 7 week old choline acetyltransferase-enhanced green fluorescent protein (ChAT-eGFP) BAC transgenic mice; transgenic mice with mitochondrial matrix targeted redox sensitive GPF (MTS-roGFP) driven by a CMV promoter (CMV-mito-roGFP mice)[12] or the latter mice crossed with *DJ-1*$^{-/-}$ mice, of both sexes, were deeply anesthetized with ketamine–xylazine and perfused transcardially with ice-cold modified artificial cerebrospinal fluid (ACSF), bubbled with 95% O_2-5% CO_2, and containing (in mM): 2.5 KCl, 26 $NaHCO_3$, 1.25 Na_2HPO_4, 0.5 $CaCl_2$, 10 $MgSO_4$, 0.4 ascorbic acid, 10 glucose, and 210 sucrose. The cerebellum, pons and medulla were rapidly removed, blocked in the coronal plane, and sectioned at a thickness of 240 μm in ice-cold modified ACSF. Slices were then submerged in ACSF, bubbled with 95% O_2-5% CO_2, and containing (in mM): 2.5 KCl, 126 NaCl, 26 $NaHCO_3$, 1.25 Na_2HPO_4, 2 $CaCl_2$, 2 $MgSO_4$, and 10 glucose, and stored at room temperature for at least one hour prior to recording and/or imaging. VTA was blocked, sectioned as described previously[12].

Slice visualization, electrophysiology and histology

The slices were transferred to the recording chamber mounted on an Olympus BX51 upright, fixed-stage microscope and perfused with oxygenated ACSF at 32 °C. A 60X, 0.9 NA water-immersion objective was used to examine the slice using standard infrared differential interference contrast video microscopy. For whole cell calcium current recordings, we used HEPES-based solutions[14]. The first solution contained (in mM): 137 NaCl, 1.8 $CaCl_2$, 1 $MgCl_2$, 5.4 tetraethylammonium (TEA)-Cl, 10 4-AP, 0.001 tetrodotoxin (TTX), 5 HEPES and 10 glucose (pH = 7.3 with NaOH), and the second solution was identical except for an equimolar substitution of $CaCl_2$ with $CoCl_2$ (pH = 7.3 with NaOH). For recording of voltage-insensitive Na+ currents we used the following two solutions[23]: the first contained (in mM): 151 NaCl, 2 $CaCl_2$, 2.5 KCl, 2 $MgCl_2$, 0.001 TTX, 5 HEPES and 10 glucose (pH = 7.3 with NaOH), and the second was identical except for a equimolar substitution of NaCl with N-methyl-D-glucamine (NMDG, pH = 7.3 with HCl).

Patch pipette resistance was typically 3–4.5 MΩ when filled with recording solution. For whole-cell current clamp recordings the pipette contained (in mM): 135.5 K-Me-SO4, 5 KCl, 2.5 NaCl, 5 Na-phosphocreatine, 10 HEPES, 0.2 EGTA, 0.21 Na_2GTP, and 2 $Mg_{1.5}ATP$ (pH=7.3 with KOH, 280–290 mOsm/kg). In some experiments, we added biocytin (5% w/v) to this internal solution. At the end of these experiments slices were fixed by immersion into 4% paraformaldehyde in 0.15 M phosphate buffer and refrigerated for a period of 2 d; reacted with streptavidin-Alexa Fluor 594 and plated for laser-scanning confocal imaging on the Olymus Fluoview FV1000 system.

For perforated patch recordings we front-filled the pipettes with the K^+-based internal solution, and back-filled with the same solution that had was sonicated after addition of 1.5

μg/ml gramicidin B. For whole cell voltage clamp recordings of calcium currents the pipette contained (in mM): 111 Cs-Me-SO_3, 12.5 CsCl, 1 $MgCl_2$, 0.1 $CaCl_2$, 10 HEPES, 1 EGTA, 0.21 Na_2GTP, and 2 $Mg_{1.5}ATP$ (pH = 7.3 with CsOH, 280–290 mOsm/kg). For calcium imaging experiments the pipette contained (in mM): 135 K-MeSO4, 5 KCl, 5 Na-phosphocreatine, 5 Tris-phosphocreatine, 10 HEPES, 0.1 Fluo-4, 0.05 Alexa Fluor 568, 0.21 Na_2GTP, and 2 $Mg_{1.5}ATP$ (pH = 7.3 with KOH, 280–290 mOsm/Kg).

Electrophysiological recordings were obtained with a Multiclamp 700B amplifier (Molecular Devices, Sunnyvale, CA). Junction potential, which was 7–8 mV, was not corrected. Signals were digitized at 20–100 kHz and logged onto a personal computer with the Clampex 9.2 software (Molecular Devices) or, in the imaging experiments, using the custom-written shareware package WinFluor (John Dempster, Strathclyde University, Glasgow, Scotland, UK), which automates and synchronizes the 2PLSM imaging and electrophysiological protocols.

2PLSM imaging

The 2PLSM system was described previously[12]. Briefly, the two-photon excitation source was a Chameleon Ultra 2 tunable laser system (680–1,080 nm) (Coherent Laser Group, Santa Clara, Ca). Optical signals were acquired using an 820-nm excitation beam to excite Alexa and Fluo-4 dyes simultaneously. Laser power attenuation was achieved with two Pockels cells electro-optic modulators (model 350-80, Conoptics, Danbury, CT). The fluorescence emission was collected with non-descanned photomultiplier tubes (PMTs) (Prairie Technologies, Madison, WI). A Dodt contrast detector system was used to provide a bright-field transmission image in registration with the fluorescent images. For the calcium buffering experiments regions of interest were chosen to cover a small rectangular patch of soma, and 20–50 Hz scans were conducted, using 0.183 μm pixels and 12 μs dwell time.

Optical imaging of roGFP signals was performed by using a 920 nm excitation beam. The two-photon excitation source was a Chameleon Ultra 2 tunable laser system (706–1,000 nm). The roGFP fluorescence (490–560 nm) was detected by a PMT. Sixty frames of the roGFP signal were collected in one optical plane at a rate of 3–5 frames per second, to determine the baseline fluorescence (F) of the cell. At the end of all experiments, 2 mM dithiothreitol (DTT) was applied for 10 min to reduce the mitochondria fully so as to measure the maximal fluorescence (F_{DTT}), followed by 100 μM Aldrithiol (Ald) for 0.75 to 1.5 h to oxidize the mitochondria fully, so as to determine the minimal fluorescence (F_{Ald}). The relative oxidation was then calculated as $(F_{DTT} - F)/(F_{DTT} - F_{Ald})$[12].

Drugs and reagents

For recording of autonomous discharge the following cocktail of synaptic receptor blockers was used that included (in μM): 50 D-APV, 5 NBQX, 10 SR 95531, 1 CGP 55845, 10 mecamylamine, 10, ketanserin and in many experiments 10 phentolamine. Voltage sensitive Na^+ channels were blocked with 1 μM TTX. Cav2.2 channels were blocked with 1 μM ω-conotoxin GVIA. Cav1 channels were antagonized acutely with 5 μM of either nifedipine or isradipine, or preincubated in 200 nM isradipine. Alternatively, 200 nM of calciseptine was used for this purpose (either acutely or with preincubation). Small conductance calcium-

activated (SK) K^+ channels were blocked with 100 nM apamin. Large conductance voltage- and calcium-activated (BK) K^+ channels were blocked with 0.5 mM TEA. HCN channels were blocked with 20 μM ZD 7288. The acute effects of solution exchanges or drug applications were measured at least 5 min after wash on, except for dihydropyridine where 10 min were given. Fluo-4 pentapotassium and Alexafluor 568/594 hydrazide Na^+ salts were obtained from Invitrogen (Carlsbad, CA). TTX, the conotoxin and calciseptine were obtained from Alomone Labs (Jerusalem, Israel). The rest of the drugs and reagents were obtained from Tocris (Ellisville, MO) or Sigma (St. Louis, MO).

Single-cell RT-PCR

In some experiments, the contents of DMV neurons in the slice were aspirated into an electrode. The electrode tip was broken in a 0.6 ml presiliconized tube (Midwest Scientific, Valley Park, MO) containing 1.9 μl of DEPC-treated water, 0.7 μl of RNaseOUT (20 U/μl), 0.7 μl of oligo-dT (50 μM),1.0 μl random hexamers (50ng/μl), 0.7 μl of BSA (143 μg/μl), 1.0 μl of dNTPs (10 mM), and the contents were ejected into the presiliconized tube, and frozen at −80°C for reverse transcription. The single-cell cDNA generated from the reverse transcription step was subjected to conventional PCR. Primers for Cav1.2, Cav1.3 and ChAT were developed in-house. Primer Nalcn mRNA (GenBank accession number is NM177393) was detected with a pair of primers, 5′-GGTGCACTCTCTGCTGCGCA (position 479) and 5′-CGCAGCATGCCCCAAGGTGA (position 796). The predicted PCR product length was 317 bp.

Estimation of endogenous buffering capacity

To estimate the endogenous buffering capacity κ_S we use the ‘added buffer method’. In this method a competition is created between endogenous buffers and the added Fluo-4 dye, whose buffering capacity is denoted κ_B, in binding to the free calcium as the dye diffuses into the cellular compartment, in our case the soma[33]. Because the time course of this diffusion (measured in minutes) is much longer than the timescale of dissociation (measured in milli-seconds), the concentration of bound exogenous buffer, [CaB], can be considered at equilibrium with [Ca], the concentration of free calcium, while the cell fills. This assumption is particularly true when the cells is quiescent and hence truly at steady-state. In this case, the law of mass action yields

$$[CaB] = \frac{[B][Ca]}{K_D + [Ca]}$$

where [B] and K_D are the concentration and the dissociation constant of the exogenous buffer Fluo-4, respectively. Differentiation of this equation with respect to time yields

$$\frac{d}{dt}[CaB] = \frac{\partial [CaB]}{\partial [Ca]}\frac{d}{dt}[Ca] + \frac{[Ca]}{K_D + [Ca]}\frac{d}{dt}[B] \quad [1]$$

The pre-factor of the first term on the right side (r.h.s.) is the definition of the binding capacity of the dye and is denoted $\kappa_B \equiv \frac{\partial[CaB]}{\partial[Ca]} = \frac{[B]K_D}{(K_D+[Ca])^2}$ and measures the number of calcium ions bound to the buffer per each free ion. The time course of the rise in [B] in the soma is quite generally exponential-shaped because the driving force of the diffusion is the difference between the concentration of the dye in the pipette $[B]_T$ and [B] so that [B] is expected to behave more or less like $[B]=[B]_T\left(1-e^{-t/\tau}\right)$ with some decay time constant τ (which in our experiment was on the order of a minute or so)[33]. Thus eq. [2] can be rewritten as

$$\frac{d}{dt}[CaB]=\kappa_B\frac{d}{dt}[Ca]+\frac{[Ca][B]_T}{K_D+[Ca]}\frac{e^{-t/\tau}}{\tau}$$

In the 'added buffer method' we take advantage of the first term in the r.h.s. of eq. [1a], and generate well-controlled perturbation in [Ca], namely by silencing the cell with hyperpolarizing currents and evoking well-spaced single spikes in the cell that are assumed to introduce a reproducible amount of calcium ions [in moles], denoted $\upsilon_{Ca^{2+}}$ into the soma, whose volume is denoted v. We can therefore write[33, 34]

$$(1+\kappa_S+\kappa_B)\frac{d}{dt}[Ca]=\frac{\upsilon_{Ca^{2+}}}{v}\sum_{t_{AP}}\delta(t-t_{AP})+\text{other terms} \quad [2]$$

where $\delta(t - t_{AP})$ is a Dirac delta function representing an impulse when the spikes occur. Substituting eq. [2] in [1] and solving eq. [1] reveals that [CaB] will undergo a stepwise increase when spikes occur superimposed on the slow dynamics described by the first term on the r.h.s. of eq. [1a]. Namely

$$[CaB]=\frac{\upsilon_{Ca^{2+}}}{v}\sum_{t_{AP}}\frac{\kappa'_B(t_{AP})}{1+\kappa_S+\kappa'_B(t_{AP})}H(t-t_{AP})+\text{other terms} \quad (3)$$

where κ'_B is the incremental binding ratio, defined below in eq. [5] and H(t-t_{AP}) is the Heaviside step function added with each spike.

Because Fluo-4 has a very high dynamic range, (i.e., $R=F_{max}/F_{min}$ is on the order of 100)[32], the brightness of the Fluo-4 dye F can be regarded as proportional to the concentration of the bound dye, i.e., $F=S_{CaB}[CaB]$. Thus, eq. [3] implies that step-like increases in the raw value of F should be observed with each spike. Importantly, because [B] rises slowly as the soma fills, the sequence of spikes will produce montonically increasing values $\kappa'_B(t_{AP})$. If we denote the resting concentration of free calcium as $[Ca]_0$, and the fluorescence corresponding to it as F_0, then the amplitude of the steps in the raw value of F induced by each spike ($\Delta F_{AP}=F_{AP} - F_0$ that corresponds to an increment in free calcium denoted ⊗

$[Ca]_{AP}$) should also increase montonically like a 'binding isotherm' and generate the following relationship between ΔF_{AP} and κ'_B

$$\Delta F_{AP} = \Delta F_{AP}^{\max} \frac{\kappa'_B}{1+\kappa_S+\kappa'_B} \quad [4]$$

Eq. [4] can be used to extract κ_S (eq. 25 in ref. 33). We estimated κ'_B by substituting the expressions they derived for $[Ca]_0$, and $\otimes$ [Ca] into the definition of the incremental binding ratio of the buffer[32] to yield the following expression

$$\kappa'_B \equiv \frac{[B]K_D}{(K_D+[Ca]_0)(K_D+[Ca]_0+\Delta[Ca]_{AP})} = \frac{[B]/K_D}{(1+df_{\max}^{-1})^2}\left(1-\frac{df_{AP}}{df_{\max}}\right) \quad [5]$$

where $df_{AP} = \frac{\Delta F_{AP}}{F_0}$.

F_0 is the value of fluorescence when the cells are quiescent[34] (in the case of pacemaking neurons such as the DMV or VTA neurons this required a constant hyperpolarizing currents). df_{max} is defined as $(F_{max} - F_0)/F_0$ and F_{max} is measured as explained below. [B] is estimated at the time F_0 is measured, from the baseline fluorescence normalized so that it approaches a steady state of the pipette concentration of Fluo-4 (i.e., 100 or 200 μM). The K_D of Fluo-4 was taken to be 345 nM. Because all buffering capacity estimates are uniformly scaled by this value, it may introduce a systematic error but will not affect comparisons among different populations[32]. Importantly, in deriving eq. [5] the 1/R term that appears in ref. 32 is neglected due to the very high dynamic range of Fluo-4.

The experiment is thus conducted as follows: a cell is patched and the 2PLSM imaging of a small rectangular patch of the soma is commenced. The seal is ruptured and then a hyperpolarizing current in injected to silence the cell. Then, on the background of this hyperpolarizing current, a series of 2 nA, 2ms pulses are injected every 10 s for 2.5–3 min to generate nominally identical and instantaneous calcium increments. The measurements of the resulting increments in raw fluorescence ΔF_{AP} in conjunction with the estimated [B] and df_{max} enable the estimation of κ'_B (eq. [5]). Using the fact that the a double reciprocal plot of eq. [4], yields a linear relation, we generated a scatter plot of $(1/\kappa'_B, 1/\Delta F_{AP})$ to estimate κ_S (which can be extracted from fitting a linear regression to the scatter plot)[33]. At the end of the experiments df_{max} was estimated as follows: a sequence of 7 s long current injections into the soma of increasing intensity, in 100 pA increments, were used in order to saturate the brightness of the fluorescence and hence the dye[34].

Data and Statistical Analysis

data were analyzed and curve fitting was done using custom-made code on custom-made (Winfluor; NUPver, Nicholas Schwarz, Northwestern University; Oscilloscope, Dr. Charles Wilson, University of Texas at San Antonio) and commercial (Mathematica 8, Wolfram Research, Champaign, IL; Matlab 7, The Mathworks, Natick, MA) software. Spike threshold was identified as the maximal dV/dt of the voltage trajectory, and the width of the

spike as measured as the time from threshold crossing to repolarization back to threshold. Nonparametric statistical tests for changes in medians were used. For independent samples the two-tailed Wilcoxon rank-sum test and Kruskal Wallis one-way ANOVA were used, and for matched pairs the two-tailed Wilcoxon signed-rank test (SRT) was used. Null hypotheses were rejected if the *P* value was below 0.05.

Supplementary Material

Refer to Web version on PubMed Central for supplementary material.

Acknowledgments

We thank Yu Chen, Sasha Ulrich, Karen Saporito and Dongjun Ren for their expert technical help. We thank Dr. Richard Miller for valuable discussions. This work was supported by grants from the Hartman Foundation, the IDP Foundation, the Picower Foundation, the NIH (P50 NS047085 and T32 NS041234) and the DoD (W81XWH-11-1-051) to D.J.S.

References

1. de Lau LM, Breteler MM. Epidemiology of Parkinson's disease. Lancet Neurol. 2006; 5:525–535. [PubMed: 16713924]
2. Biskup S, Moore DJ. Detrimental deletions: mitochondria, aging and Parkinson's disease. Bioessays. 2006; 28:963–967. [PubMed: 16998822]
3. Lees AJ, Hardy J, Revesz T. Parkinson's disease. Lancet. 2009; 373:2055–2066. [PubMed: 19524782]
4. Schapira AH. Mitochondria in the aetiology and pathogenesis of Parkinson's disease. Lancet Neurol. 2008; 7:97–109. [PubMed: 18093566]
5. Albin RL, Young AB, Penney JB. The functional anatomy of disorders of the basal ganglia. Trends Neurosci. 1995; 18:63–64. [PubMed: 7537410]
6. Jellinger KA. A critical reappraisal of current staging of Lewy-related pathology in human brain. Acta Neuropathol. 2008; 116:1–16. [PubMed: 18592254]
7. Braak H, Ghebremedhin E, Rub U, Bratzke H, Del Tredici K. Stages in the development of Parkinson's disease-related pathology. Cell Tissue Res. 2004; 318:121–134. [PubMed: 15338272]
8. Dickson DW, et al. Evidence that incidental Lewy body disease is pre-symptomatic Parkinson's disease. Acta Neuropathol. 2008; 115:437–444. [PubMed: 18264713]
9. Surmeier DJ, Guzman JN, Sanchez-Padilla J, Goldberg JA. The origins of oxidant stress in Parkinson's disease and therapeutic strategies. Antioxid Redox Signal. 2011; 14:1289–1301. [PubMed: 20712409]
10. Sulzer D. Multiple hit hypotheses for dopamine neuron loss in Parkinson's disease. Trends Neurosci. 2007; 30:244–250. [PubMed: 17418429]
11. Grace AA, Bunney BS. The control of firing pattern in nigral dopamine neurons: single spike firing. J Neurosci. 1984; 4:2866–2876. [PubMed: 6150070]
12. Guzman JN, et al. Oxidant stress evoked by pacemaking in dopaminergic neurons is attenuated by DJ-1. Nature. 2010; 468:696–700. [PubMed: 21068725]
13. Nedergaard S, Flatman JA, Engberg I. Nifedipine- and omega-conotoxin-sensitive Ca2+ conductances in guinea-pig substantia nigra pars compacta neurones. J Physiol. 1993; 466:727–747. [PubMed: 8410714]
14. Puopolo M, Raviola E, Bean BP. Roles of subthreshold calcium current and sodium current in spontaneous firing of mouse midbrain dopamine neurons. J Neurosci. 2007; 27:645–656. [PubMed: 17234596]
15. Foehring RC, Zhang XF, Lee JC, Callaway JC. Endogenous calcium buffering capacity of substantia nigral dopamine neurons. J Neurophysiol. 2009; 102:2326–2333. [PubMed: 19675297]

16. Ilijic E, Guzman JN, Surmeier DJ. The L-type channel antagonist isradipine is neuroprotective in a mouse model of Parkinson's disease. Neurobiol Dis. 2011; 43:364–371. [PubMed: 21515375]
17. Natale G, Pasquali L, Ruggieri S, Paparelli A, Fornai F. Parkinson's disease and the gut: a well known clinical association in need of an effective cure and explanation. Neurogastroenterol Motil. 2008; 20:741–749. [PubMed: 18557892]
18. Miller VM, et al. Dorsal motor nucleus of vagus protein aggregates in Lewy body disease with autonomic dysfunction. Brain Res. 2009; 1286:165–173. [PubMed: 19501577]
19. Gao H, et al. Morphological and electrophysiological features of motor neurons and putative interneurons in the dorsal vagal complex of rats and mice. Brain Res. 2009; 1291:40–52. [PubMed: 19619517]
20. Mo ZL, Katafuchi T, Muratani H, Hori T. Effects of vasopressin and angiotensin II on neurones in the rat dorsal motor nucleus of the vagus, in vitro. J Physiol. 1992; 458:561–577. [PubMed: 1302279]
21. Travagli RA, Gillis RA. Hyperpolarization-activated currents, IH and IKIR, in rat dorsal motor nucleus of the vagus neurons in vitro. J Neurophysiol. 1994; 71:1308–1317. [PubMed: 8035216]
22. Bean BP. The action potential in mammalian central neurons. Nat Rev Neurosci. 2007; 8:451–465. [PubMed: 17514198]
23. Khaliq ZM, Bean BP. Pacemaking in dopaminergic ventral tegmental area neurons: depolarizing drive from background and voltage-dependent sodium conductances. J Neurosci. 2010; 30:7401–7413. [PubMed: 20505107]
24. Lu B, et al. The neuronal channel NALCN contributes resting sodium permeability and is required for normal respiratory rhythm. Cell. 2007; 129:371–383. [PubMed: 17448995]
25. Putzier I, Kullmann PH, Horn JP, Levitan ES. Cav1.3 channel voltage dependence, not Ca2+ selectivity, drives pacemaker activity and amplifies bursts in nigral dopamine neurons. J Neurosci. 2009; 29:15414–15419. [PubMed: 20007466]
26. Guzman JN, Sanchez-Padilla J, Chan CS, Surmeier DJ. Robust pacemaking in substantia nigra dopaminergic neurons. J Neurosci. 2009; 29:11011–11019. [PubMed: 19726659]
27. Koschak A, et al. alpha 1D (Cav1.3) subunits can form l-type Ca2+ channels activating at negative voltages. J Biol Chem. 2001; 276:22100–22106. [PubMed: 11285265]
28. Hocherman SD, Werman R, Yarom Y. An analysis of the long-lasting after-hyperpolarization of guinea-pig vagal motoneurones. J Physiol. 1992; 456:325–349. [PubMed: 1293279]
29. Sah P, McLachlan EM. Ca(2+)-activated K+ currents underlying the afterhyperpolarization in guinea pig vagal neurons: a role for Ca(2+)-activated Ca2+ release. Neuron. 1991; 7:257–264. [PubMed: 1873029]
30. von Lewinski F, Keller BU. Ca2+, mitochondria and selective motoneuron vulnerability: implications for ALS. Trends Neurosci. 2005; 28:494–500. [PubMed: 16026864]
31. de Leon M, Covenas R, Narvaez JA, Aguirre JA, Gonzalez-Baron S. Distribution of parvalbumin immunoreactivity in the cat brain stem. Brain Res Bull. 1993; 32:639–646. [PubMed: 8221163]
32. Maravall M, Mainen ZF, Sabatini BL, Svoboda K. Estimating intracellular calcium concentrations and buffering without wavelength ratioing. Biophys J. 2000; 78:2655–2667. [PubMed: 10777761]
33. Neher E, Augustine GJ. Calcium gradients and buffers in bovine chromaffin cells. J Physiol. 1992; 450:273–301. [PubMed: 1331424]
34. Helmchen F, Imoto K, Sakmann B. Ca2+ buffering and action potential-evoked Ca2+ signaling in dendrites of pyramidal neurons. Biophys J. 1996; 70:1069–1081. [PubMed: 8789126]
35. Lips MB, Keller BU. Activity-related calcium dynamics in motoneurons of the nucleus hypoglossus from mouse. J Neurophysiol. 1999; 82:2936–2946. [PubMed: 10601430]
36. Lang DG, Ritchie AK. Tetraethylammonium blockade of apamin-sensitive and insensitive Ca2(+)-activated K+ channels in a pituitary cell line. J Physiol. 1990; 425:117–132. [PubMed: 1698974]
37. Kahle PJ, Waak J, Gasser T. DJ-1 and prevention of oxidative stress in Parkinson's disease and other age-related disorders. Free Radic Biol Med. 2009; 47:1354–1361. [PubMed: 19686841]
38. Mercuri NB, Bonci A, Calabresi P, Stefani A, Bernardi G. Properties of the hyperpolarization-activated cation current Ih in rat midbrain dopaminergic neurons. Eur J Neurosci. 1995; 7:462–469. [PubMed: 7773443]

39. Helton TD, Xu W, Lipscombe D. Neuronal L-type calcium channels open quickly and are inhibited slowly. J Neurosci. 2005; 25:10247–10251. [PubMed: 16267232]
40. Dooley CT, et al. Imaging dynamic redox changes in mammalian cells with green fluorescent protein indicators. J Biol Chem. 2004; 279:22284–22293. [PubMed: 14985369]
41. Nicholls DG, Budd SL. Mitochondria and neuronal survival. Physiol Rev. 2000; 80:315–360. [PubMed: 10617771]
42. Yi M, Weaver D, Hajnoczky G. Control of mitochondrial motility and distribution by the calcium signal: a homeostatic circuit. J Cell Biol. 2004; 167:661–672. [PubMed: 15545319]
43. Brown GC. Control of respiration and ATP synthesis in mammalian mitochondria and cells. Biochem J. 1992; 284 (Pt 1):1–13. [PubMed: 1599389]
44. Bohnen NI, Albin RL. The cholinergic system and Parkinson disease. Behav Brain Res. 2011; 221:564–573. [PubMed: 20060022]
45. Meissner WG, et al. Priorities in Parkinson's disease research. Nat Rev Drug Discov. 2011; 10:377–393. [PubMed: 21532567]
46. Becker C, Jick SS, Meier CR. Use of antihypertensives and the risk of Parkinson disease. Neurology. 2008; 70:1438–1444. [PubMed: 18256367]
47. Ritz B, et al. L-type calcium channel blockers and Parkinson disease in Denmark. Ann Neurol. 2010; 67:600–606. [PubMed: 20437557]
48. Pasternak B, et al. Use of calcium channel blockers and Parkinson's disease. Am J Epidemiol. 2012; 175:627–635. [PubMed: 22387374]
49. Marras C, et al. Dihydropyridine calcium channel blockers and the progression of parkinsonism. Ann Neurol. 2012; 71:362–369. [PubMed: 22451203]
50. Hirsch EC, Hunot S. Neuroinflammation in Parkinson's disease: a target for neuroprotection? Lancet Neurol. 2009; 8:382–397. [PubMed: 19296921]

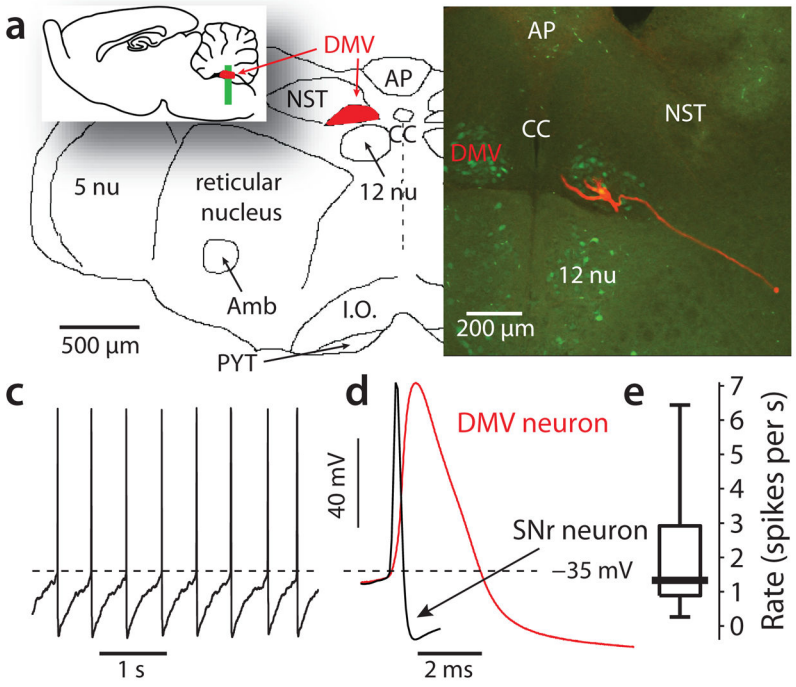

Figure 1.

Autonomous discharge in cholinergic neurons of the dorsal motor nucleus of the Vagus (DMV). (a) the DMV is located in the medulla oblongata dorsal to the hypoglossal nucleus (12 nu) and lateral to the central canal (CC). inset: sagittal view. Abbreviations: 5 nu – trigeminal nucleus, Amb – nucleus ambiguus, AP – area postrema, I.O. – inferior olive, NST – nucleus of the solitary tract, PYT – pyramidal tract. (b) a confocal image of a transverse slice of the medulla from a ChaT-eGFP mouse (approximate location indicated in inset of panel a). Bilateral DMV can be seen lateral to the central canal and dorsal to the hypoglossal nucleus. The overwhelming majority of neurons in the DMV are ChAT positive. One such cell was filled with biocytin and reacted with streptavidin-Alexafluor 594. Dendrites and a ventrolaterally coursing axon are visible. (c) perforated patch recording of the autonomous discharge in a DMV neuron in the presence of a cocktail of synaptic blockers. (d) waveform of an spike of a DMV neuron (red). An spike from a GABAergic neuron of the substantia nigra pars reticulata (SNr) is shown for comparison (black). (e) distribution of the autonomous firing rates of DMV neurons in the presence of the blockers.

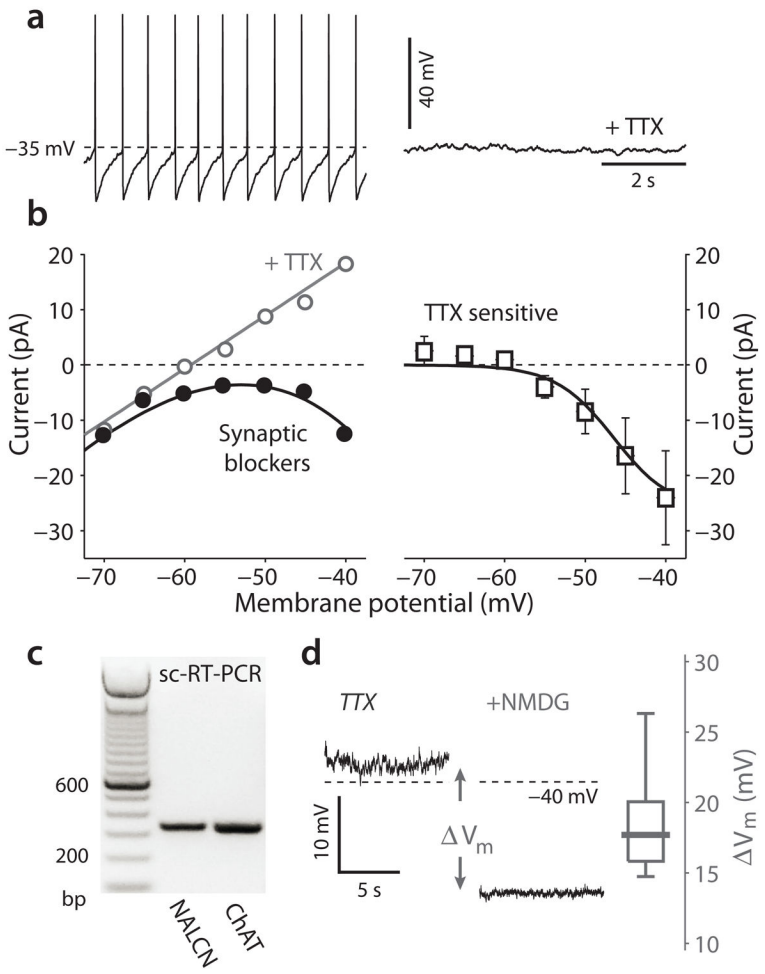

Figure 2.

Role of sodium currents in the pacemaking of cholinergic DMV neurons. (**a**) a perforated patch recording from a cholinergic DMV neuron during pacemaking in the presence of a cocktail of synaptic blockers before and after application of 1 μM tetrodotoxin (TTX). (**b**) *left*: steady-state I-V curve of a DMV neuron before (black) and after (gray) TTX application. *right*: population average (mean ± sem) of the persistent TTX sensitive currents. Solid line: fit of a Boltzman sigmoidal curve for conductance multiplied by an electromotive force with a sodium Nernst potential of +70 mV, which is the predicted empirical potential. (**c**) single-cell reverse transcription PCR (sc-RT-PCR) reveals the presence of the NALCN channel mRNA in 6/10 of the cholinergic in DMV neurons. (**d**) recording of the TTX-induced stable resting potential before and after total sodium replacement with N-methyl-D-glucamine (NMDG) reveals a large hyperpolarization. The distribution of NMDG-induced hyperpolarizations (ΔV_m) is shown on the right.

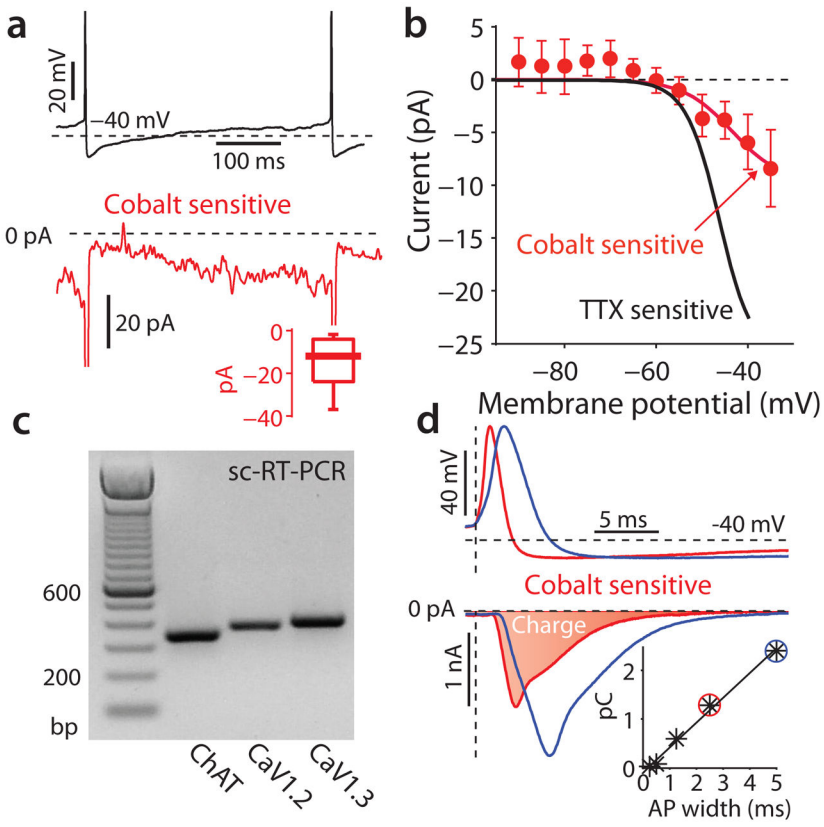

Figure 3.

Calcium currents during the pacemaking cycle in DMV neurons. (**a**) cobalt-sensitive calcium currents recorded (bottom) in response to a voltage clamped spike waveform recorded from a DMV neuron (top). Inset: distribution of the cobalt-sensitive subthreshold calcium current measured prior to the spike. (**b**) population average (mean ± sem) of the persistent cobalt-sensitive calcium currents as a function of voltage. Solid red line is a fit as in Fig. 2c, but with a calcium Nernst potential of +120 mV. The fit for the TTX sensitive current from Fig. 2c is shown in black for comparison. (**a**) single-cell reverse transcription PCR (sc-RT-PCR) reveals the presence of mRNA for Cav1.2 and Cav1.3 channels in DMV cholinergic neurons (in 7/8 and 3/8 cells, respectively). (**d**) cobalt-sensitive calcium action currents generated by a physiological spike (red) and one expanded to twice the duration (blue). Vertical dashed line is the time of spike threshold, as determined by maximal *dV/dt*. Inset: calcium charge (=shaded area) as a function of spike duration.

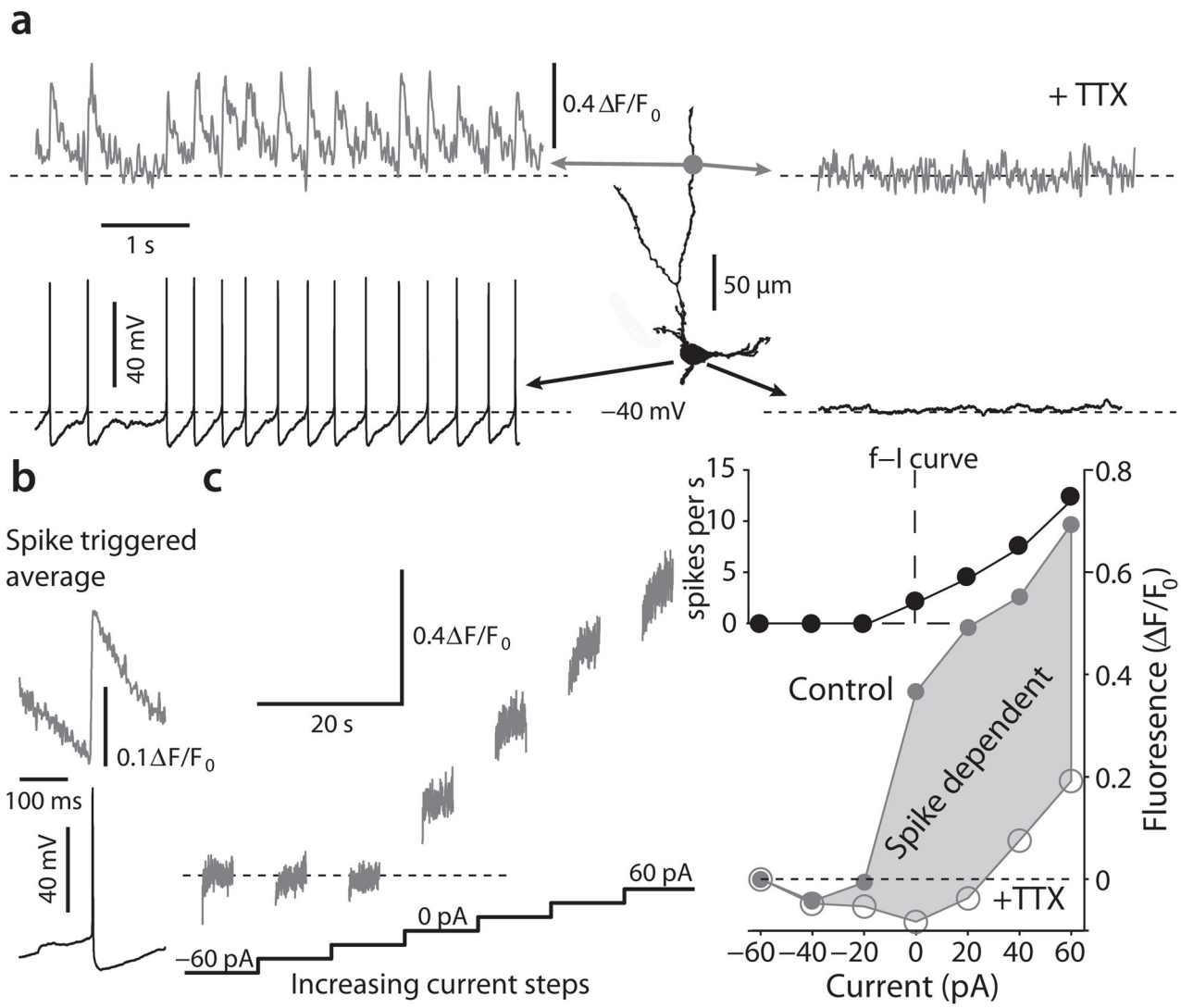

Figure 4.

2PLSM calcium imaging demonstrates that calcium dynamics are dominated by spike associated influx. (**a**) *Left*: Somatic voltage recording and 2PLSM Fluo-4 imaging from a distal dendritic location (140 µm from soma) of a DMV cell reveal spontaneous discharge that is accompanied by spike associated calcium transients. *Right*: Application of TTX reveals a stable resting potential without any subthreshold calcium oscillations. (**b**) spike triggered average of calcium transients in a DMV neuron reveal a rapid increase in calcium that is followed by an exponential decay. (**c**) *Left*: 2PLSM calcium imaging from the soma in response to a sequence of 10-s current injections from −60 pA to +60 pA to either hyperpolarize and silence discharge or to depolarize and increase discharge. The value of fluorescence for 0 pA is defined as the *ambient* fluorescence. *Right*: bottom – the plot of fluorescence as a function of current before (filled circles) and after (empty circles) TTX treatment demonstrates that the majority of calcium entry is spike-dependent. At the population level, the rise in free calcium as a function of applied current, estimated from the slope of this function from −20 to +60 pA, decreased significantly in TTX (not shown, $n = 6$

cells, $P < 0.05$, SRT). top – frequency-intensity (f–I) curve of this neuron in response to the same current steps.

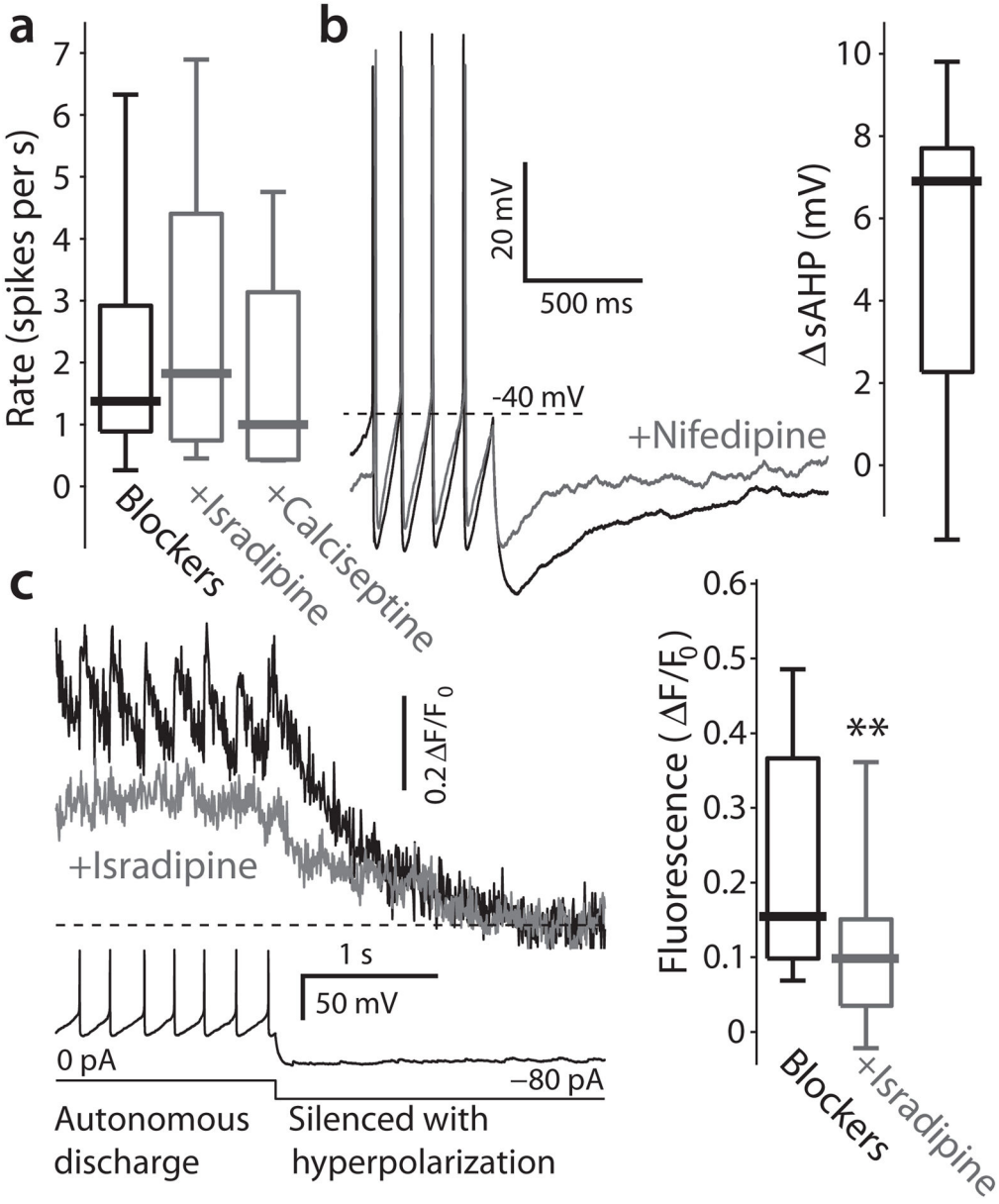

Figure 5.

Contribution of Cav1 channels to discharge patterns and ambient calcium levels in DMV neurons. (**a**) Preincubation in 200 nM of either isradipine or calciseptine, that antagonize Cav1 channels, does not alter the distribution of DMV neurons firing rates. (**b**) Application of 5 μM nifedipine, a Cav1 channel antagonist, significantly reduced the depth of the slow afterhyperpolarization (sAHP), measured from spike threshold, that follows long depolarizing pulses. Inset: distribution of changes in sAHP amplitude (ΔsAHP) in response to this drug. (**c**) *Left*: recording of spontaneous discharge followed by a hyperpolarizing pulse to silence the cell (*bottom*) can be used to measure the ambient fluorescence during autonomous discharge (*top*). Treatment with 5 μM isradipine consistently reduces the

baseline level of fluorescence in cholinergic DMV neurons. *Right*: distribution of ambient levels of fluorescence before and after treatment with 5 μM isradipine ** $P < 0.01$, SRT.

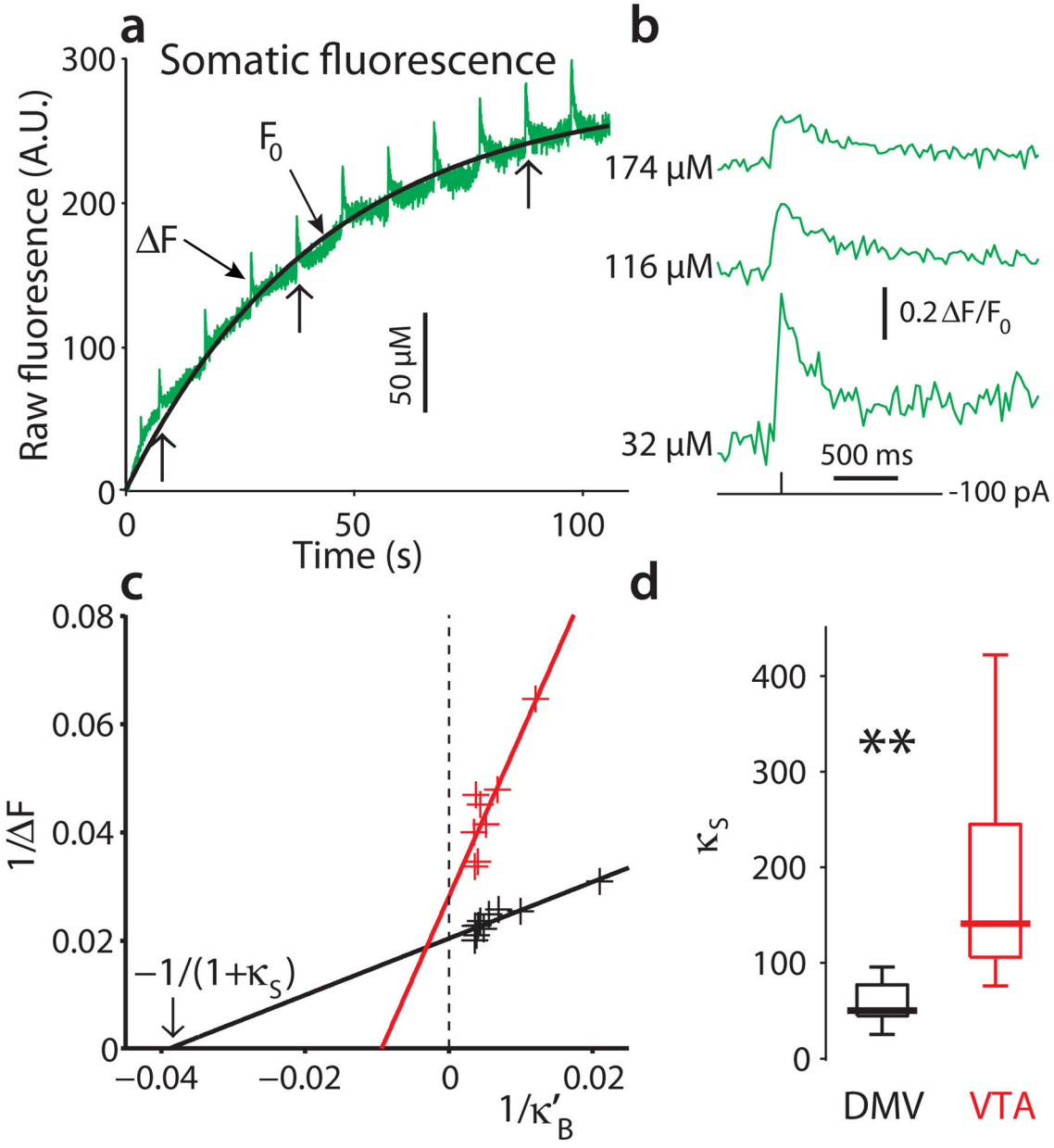

Figure 6.

DMV neurons have a low endogenous buffering capacity relative to dopaminergic VTA neurons. (**a**) Raw fluorescence as a function of time (green). Brief depolarizing pulses (2 nA, 2 ms) are delivered every 10 s for 2 min to induce an spike as the cell fills with the Fluo-4 indicator. These spikes are accompanied by brief steps in raw fluorescence (Δ*F*). Prior to these pulses and between them the cell is silenced with a constant hyperpolarizing current. Fitting an exponential curve to the temporal profile of basal fluorescence (F_0), can be used to estimate the cytosolic concentration of the Fluo-4 dye as a function of time (black). A.U. – arbitrary units. (**b**) Spike induced transients in free cytosolic calcium concentration, measured with $\Delta F/F_0$, decrease and get prolonged as the concentration of the added buffer increases (data excised from around the points marked with vertical arrows in panel **a**). (**c**)

Fitting a linear regression line to the scatter plot of the reciprocal of ΔF as a function of the reciprocal of the incremental buffering capacity κ'_B (see Online Methods) for one DMV neuron (black) and one dopaminergic neuron of the ventral tegmental area (VTA, red) yields estimates of the endogenous buffering capacity (κ_S) in these cells. (**d**) the distribution of κ_S for both populations is shown on the right, demonstrating that the buffering capacity of DMV neurons is significantly smaller than that of dopaminergic VTA neurons (** $P <$ 0.005, RST).

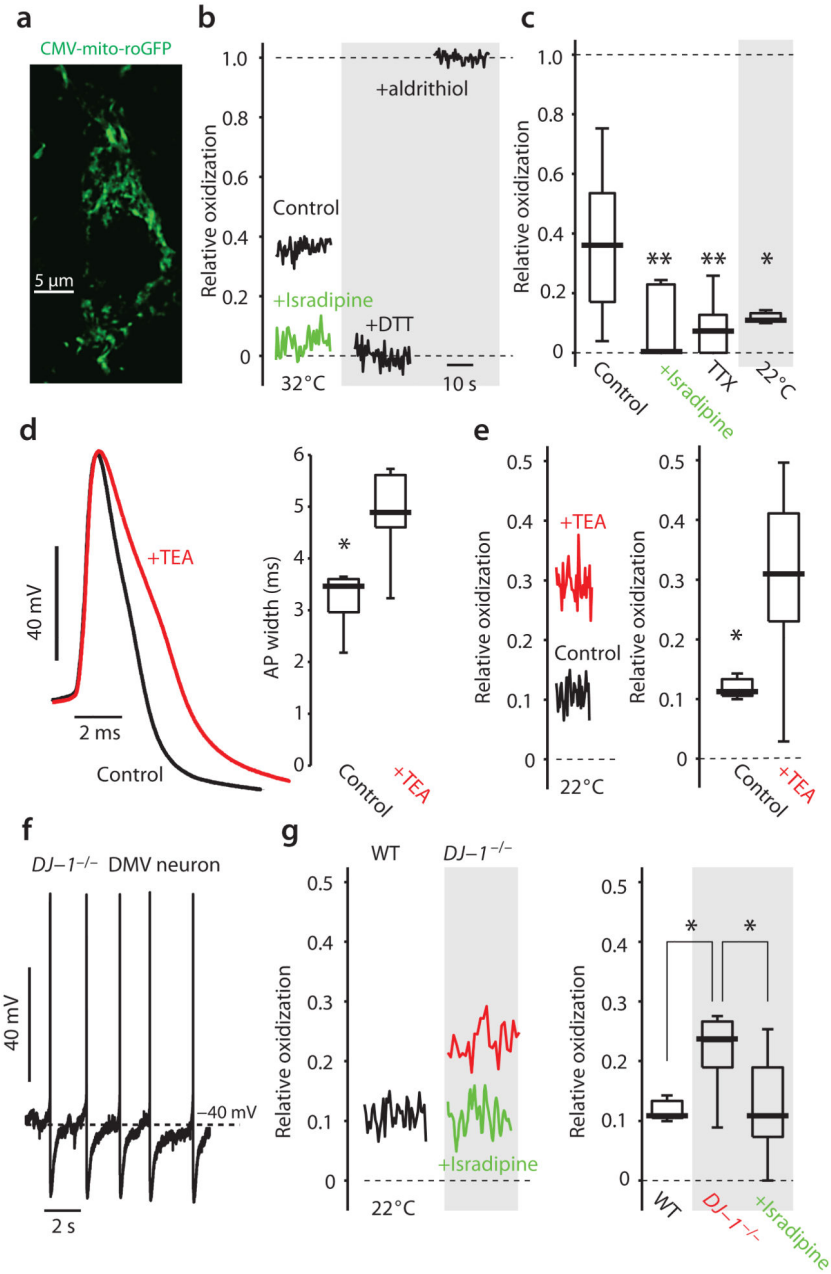

Figure 7.

Mitochondria in DMV neurons are normally oxidized and are reduced by preincubation in isradipine. (**a**) A confocal image of the soma and proximal dendrite of a DMV neuron from a CMV-mito-roGFP mouse. (**b**) The relative oxidization is estimated by measuring the resting fluorescence of the mitochondria relative to post-treatment with strong reducing (dithiothreitol, DTT) and oxidizing (aldritihiol) agents. Preincubation in 200 nM isradipine reduces the cells (green). (**c**) DMV neurons exhibit a broad range of relative oxidization. Pre-incubation in 200 nM isradipine or 1 µM TTX reduces the mitochondria matrix proteins, as does lowering the bath temperature to 22 °C. (**d**) bath application of 0.5 mM TEA significantly and reversibly (not shown) broadened the spike in every DMV neurons

recorded. (**e**) Pre-incubation in 0.5 mM TEA significantly oxidized the mitochondria (red). (**f**) Autonomous discharge of a DMV neuron from CMV-mito-roGFP mice lacking the *DJ-1* gene (*DJ-1*$^{-/-}$). (**g**) The basal oxidation of mitochondrial matrix proteins was significantly higher in *DJ-1*$^{-/-}$ mice. Pre-incubation in 200 nM isradipine significantly reduced the mitochondria of DMV cells in these animals. ** P <0.01, * P < 0.05, RST.